INL/JOU-15-35835
Accepted Manuscript

Frequency-resolved Raman for Transient Thermal Probing and Thermal Diffusivity Measurement

TIANYU WANG, SHEN XU,
DAVID H. HURLEY, YANAN YUE,
XINWEI WANG

January 2016

The INL is a
U.S. Department of Energy
National Laboratory
operated by
Battelle Energy Alliance

This is an accepted manuscript of a paper intended for publication in a journal. This document was prepared as an account of work sponsored by an agency of the United States Government. Neither the United States Government nor any agency thereof, or any of their employees, makes any warranty, expressed or implied, or assumes any legal liability or responsibility for any third party's use, or the results of such use, of any information, apparatus, product or process disclosed in this report, or represents that its use by such third party would not infringe privately owned rights. The views expressed in this paper are not necessarily those of the United States Government or the sponsoring agency.

Prepared for the U.S. Department of Energy
Office of Nuclear Energy
Under DOE Idaho Operations Office
Contract DE-AC07-05ID14517

Frequency-resolved Raman for Transient Thermal Probing and Thermal Diffusivity Measurement

TIANYU WANG,[1,4] SHEN XU,[1,4] DAVID H. HURLEY,[2,*] YANAN YUE,[3] XINWEI WANG,[1,*]

[1]*Department of Mechanical Engineering, Iowa State University, Ames, Iowa 50010, USA*
[2]*Idaho National Laboratory, Idaho Falls, Idaho 83415*
[3]*School of Power and Mechanical Engineering, Wuhan University, Wuhan, Hubei, PR China*
[4]*These authors contributed equally*
**Corresponding author: david.hurley@inl.gov and xwang3@iastate.edu*

Received XX Month XXXX; revised XX Month, XXXX; accepted XX Month XXXX; posted XX Month XXXX (Doc. ID XXXXX); published XX Month XXXX

A new transient Raman thermal probing technique: frequency-resolved Raman (FR-Raman) is developed for probing the transient thermal response of materials and measuring their thermal diffusivity. The FR-Raman uses an amplitude modulated square-wave laser for simultaneous material heating and Raman excitation. The evolution profile of Raman properties: intensity, Raman wavenumber, and emission, against frequency are reconstructed and used for fitting to determine the thermal diffusivity. A microscale Si cantilever is used to investigate the capacity of this new technique. The thermal diffusivity is determined as 9.57×10^{-5} m^2/s, 11.00×10^{-5} m^2/s and 9.02×10^{-5} m^2/s, agreeing well with literature values. The FR-Raman provides a novel way for transient thermal probing with very high temporal resolution and μm-scale spatial resolution.

OCIS codes: *(290.5860) Scattering, Raman; (120.6780) Temperature; (120.6810) Thermal effects; (120.3940) Metrology*

http://dx.doi.org/10.1364/OL.99.099999

Micro-Raman thermometry has proved to be a reliable non-contact technique for characterizing the temperature of devices and structures with a high spatial resolution (~μm) [1,2]. By using micro-Raman spectroscopy, Beechem *et al.* mapped the temperature and stress distribution simultaneously in doped polysilicon microheaters [3]. Yue *et al.* measured the temperature rise of Si at a sub-10 nm scale induced by the nanoscale near-field laser heating [4]. Tang *et al.* investigated the temperature rise and thermal stress in a nanoscale region of a Si substrate beneath silica particles and a glass fiber [5,6]. Micro-Raman thermometry makes it possible to extract thermal physical properties, such as thermal conductivity and thermal diffusivity, from the temperature-dependent change in Raman spectrum [7]. With the help of micro-Raman spectroscopy, Chen *et al.* investigated the isotope effects on the thermal conductivity of graphene [8].

However, the application of the above Raman-based technique requires the building of a relationship between temperature and Raman spectrum by calibration. Additionally, this technique is affected by the error related to inaccurate estimation or measurement of laser energy absorption. To overcome the disadvantages mentioned above, but at the same time take advantage of the high spatial resolution of micro-Raman spectroscopy, in the past, we have developed a Time-domain Differential Raman (TD-Raman) technique to realize transient heating and simultaneous thermal probing [9]. In TD-Raman, the laser beam is modulated to square-shape pulses, whose duration is varied to track the temperature evolution. The pulse-to-pulse separation is set very large and constant, allowing completely cooling of the material before the second pulse is fired. This avoids pulse-to-pulse energy coupling and eases physical model development. On the other hand, the TD-Raman faces a significant problem in extremely short time heating and thermal probing. When the heating time is short, e.g, 20 μs, the heating/probing takes a very small portion (around 0.3%) of the overall experimental time. Even under a significantly long integration time, the Raman signal is still very weak and carries too much noise. This makes it very challenging to study very fast thermal transport phenomena: faster than 20 μs, not mentioning μs or ns scale.

In this work, we developed a "Frequency-resolved Raman" (FR-Raman) technique to overcome the significant drawback of TD-Raman on very short-time scale thermal probing, while still provides the same unique capacity in characterizing thermal transport without temperature coefficient calibration. In our FR-Raman, the thermal coupling between laser pulses has been taken into consideration, allowing us to exactly extract the thermal behavior of materials at μs scale or shorter. Also the Raman integration time can be kept short while the signal-to-noise ratio is not scarified. The FR-Raman features significant advantages over the TD-Raman in extremely fast transient thermal probing. In this work, we push the resolution to 5 μs. However, this limit can be extended further to the scale of μs and ns, fully depending on the laser modulation capacity.

Figure 1 shows the physical principle of the FR-Raman. An amplitude modulated square-wave laser with different frequencies (f) is employed to heat the sample and excite Raman signals simultaneously (Fig. 1). After a sufficient number of heating cycles, the temperature evolution of the sample becomes periodic. This warm-up

time is short and can be neglected compared to the total laser irradiation cycles used in the experiment. As shown in Fig. 1a, for a modulated square-wave laser, the laser excitation time (t_e) is equal to the thermal relaxation time (t_r). During the laser excitation time, the temperature increases continually. The temperature of the sample has a character that is similar in form to an RC integration circuit. With the temperature rise, the Raman intensity (I) decreases, the Raman wavenumber (ω) softens and linewidth (Γ) broadens. These parameters have a decreasing changing rate as the temperature changing rate keeps decreasing in the excitation time. The Raman signal is acquired during the laser excitation time. It reflects the time integral of temperature evolution during the heating period.

The variation of temperature in the laser excitation time, including the initial temperature (of the period) and the final temperature (at the end of heating time), is f-dependent. To illustrate this effect, two extreme cases (very high f and very low f) are given in Figs. 1b and 1c. Under very high f (Fig. 1b), the temperature rise in the excitation time and the temperature fall in the thermal relaxation time are very small and they are almost negligible. As a result, the sample can be thought of staying at a constant temperature in the whole process. Here, we name this state as "quasi-steady state" and its temperature is T_{qs}. Under very low f (Fig. 1c), the temperature in the laser excitation time rises from the room temperature to a steady-state temperature T_s. Thus, the temperature evolution in the laser excitation time can be divided into two periods, the transient period (t_t) and the steady state period (t_s) as shown in Fig. 1c. In this case, the transient period (t_t) is far smaller than the steady state period (t_s) and the existence of the transient period can be neglected. Therefore, temperature can be regarded as constant with a value of T_s during the excitation time. The sample at this thermal state is named as "steady state". Instead of absolute temperature, the temperature rise θ is a more useful to characterize the laser heating effect. By subtracting the room temperature T_r, we can get the temperature rise at quasi-steady state and steady state respectively, which is $\theta_{qs}=T_{qs}-T_r$ and $\theta_s=T_s-T_r$. The relation between θ_{qs} and θ_s can be readily proved as $\theta_{qs}=\theta_s/2$.

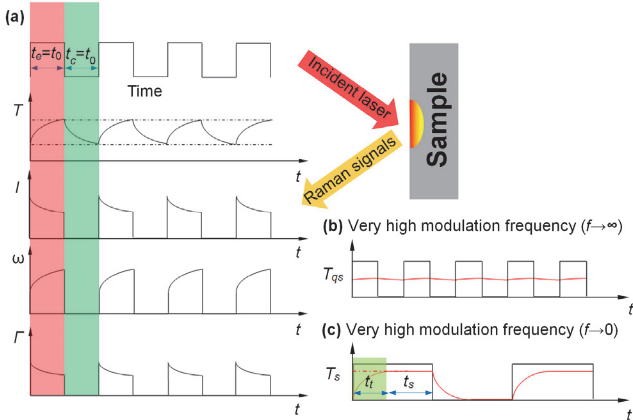

Fig. 1 (a) The concept and physics of FR-Raman. (b) The quasi-steady state under very high f. (c) The steady-state under very low f.

The Raman signals are frequency-dependent; therefore, the intensity, wavenumber and linewidth, vary from the quasi-steady to the steady state cases. It can be predicted that the Raman signals will have a decreasing intensity, a wavenumber red-shift and a linewidth broadening with decreasing f. This phenomenon is attributed to the increasing heating effect with decreasing f. The f-related variation of Raman intensity, Raman wavenumber and linewidth is determined by the thermal physical properties of sample, such as thermal diffusivity. Thus, by fitting these data with a physical model, the thermal diffusivity can be determined.

The experiment is performed on a tipless Si AFM cantilever (AppNano, Ltd) in open air at room temperature (293K). Figure 2a shows a top view of the tipless Si cantilever and its size. A continuous wave (CW) laser (MSL-III-532-AOM-150mW, Ultralaser, Inc) is amplitude modulated using a function generator (DS345). The temporal profile of the laser is that of a square-wave with a rise time of 130 ns. It is integrated into the original optical path of a commercial confocal Raman system (Voyage, B&W Tek, Inc, and Olympus BX 51). The modulated laser beam is focused by a 4× objective lens to a spot size of 31.4×65.3 μm². To heat the Si cantilever tip but at same time minimize the thermal stress and avoid the possible material damage, a low laser power of 7.9 mW (before modulation) is used. The Si cantilever is positioned using a 3D nanostage (5 nm resolution). To obtain Raman signals with a high signal-to-noise ratio, an integration time of 15 s is used. A f range from 100 kHz to 17 Hz is sufficient to capture the quasi-steady state and steady state response. Figure 2b gives several examples of Si Raman peaks at different f.

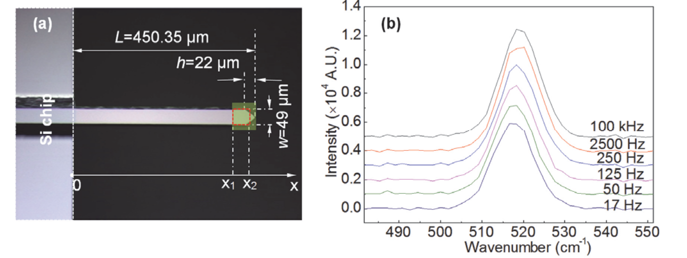

Fig. 2 (a) The optical image of tipless Si cantilever used in the experimental. The green area is the laser spot. The laser heating area is marked by red dashlines. (b) Typical Si Raman peaks at selected f.

Figure 3a shows the contour map of Si Raman peak at ~520 cm⁻¹ from 17 Hz to 100 kHz. This is intended to give an overall picture on how the Raman spectrum varies with the f. When f decreases, the Raman intensity decreases and wavenumber has a red-shift. Unlike Raman intensity and wavenumber, the variation of linewidth against f cannot be observed clearly in the contour map. Figure 3b show the numerical variation of Raman intensity, wavenumber and linewidth against f. The decreasing variation of linewidth against increasing modulation frequency can be observed, but the linewidth data exhibits a poor signal to noise ratio.

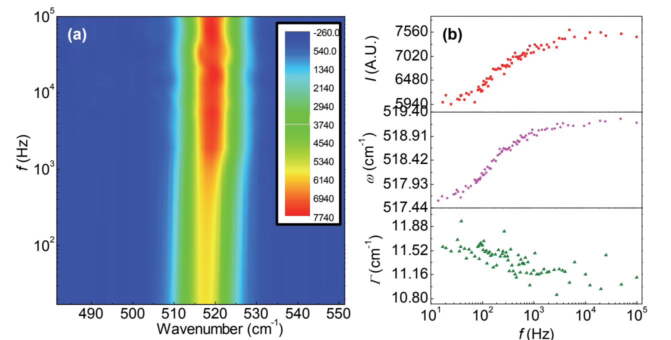

Fig. 3 (a) The contour map of Si Raman peaks. (b) The variation of Raman peak intensity, Raman wavenumber and linewidth against f.

To obtain accurate values of intensity, wavenumber and linewidth, the peaks are fitted using a Gaussian distribution function. The fitted variation of Raman intensity, wavenumber and linewidth against the modulation frequency (f) are used to extract thermal diffusivity. How fast or slow these Raman spectrum properties change from the steady state to the quasi-steady state is determined by the thermal diffusivity of the sample. To fit these properties and extract the thermal diffusivity

of Si, a physical model is developed.

To simplify the thermal transport model, a shape refined cantilever with a rectangular tip end is used to derive the temperature evolution solution. The thermal transport along the axial direction of the Si cantilever is described by one-dimensional heat conduction. The spatially averaged temperature rise of the heating area induced by the modulated square-wave laser is given by the following equation

$$\overline{\theta}(t)_{pulse} = C_0 \sum_{m=1}^{\infty} C_m [1 - e^{-m^2\pi^2\alpha t/4l^2} / (1 + e^{-m^2\pi^2\alpha/(8f_0 l^2)})] \ , \qquad (1)$$

in which $C_m = \left\{[1-(-1)^m]\cos[m\pi x_1/(2l)]\right\}^2 / (m^4\pi^4)$ and $C_0 = 8\dot{g}l^3 / [(l-x_1)k]$.

In this expression, $l=L-h/2$ and it is the length of shaped refined Si cantilever. x_1=418.95 μm and $x_2=l$=438.88 μm gives the laser heating area in the X coordinate. $\dot{g}$ represents the laser heating source. k and α is the thermal conductivity and thermal diffusivity of Si respectively. f_0 is the laser modulation frequency.

The maximum spatially averaged temperature rise $\overline{\theta}_{pulse_max}$ can be determined from this equation when $t=1/(2f_0)$ and $1/(2f_0)$ approaches infinity ($t_0 \to \infty$). The $\overline{\theta}_{pulse_max}$ is used as the reference to normalize $\overline{\theta}(t)_{pulse}$. The normalized spatially averaged temperature rise is

$$\overline{\theta}(t)_{nor} = \sum_{m=1}^{\infty} C_m [1 - e^{-m^2\pi^2\alpha t/4l^2} / (1 + e^{-m^2\pi^2\alpha/(8f_0 l^2)})] / \sum_{m=1}^{\infty} C_m \qquad (2)$$

The Raman signal $[I(\omega)]$ at any instant in the laser excitation time has a Gaussian distribution as

$$I(\omega) = A_t \exp\left[-4\ln 2 \cdot (\omega - \omega_t)^2 / \Gamma_t^2\right] \qquad (3)$$

A_t is the Raman peak intensity at the peak frequency ω_t, and Γ_t is the Raman linewidth. Parameters A_t, ω_t and Γ_t are linear functions of the normalized temperature rise in a moderate temperature range: $A_t = A_0(1 - A\overline{\theta}_{nor})$, $\omega_t = \omega_0 - B\overline{\theta}_{nor}$ and $\Gamma_t = \Gamma_0 + C\overline{\theta}_{nor}$. A_0, ω_0 and Γ_0 are Raman intensity, frequency and linewidth when the Si cantilever has no temperature rise over room temperature. A_0 is the multiple relating the theoretical normalized Raman intensity $(1 - A\overline{\theta}_{nor})$ to the experimental data. A, B and C give the total variation of normalized Raman intensity, Raman wavenumber and linewidth from the steady state to the room temperature state. To obtain the overall Raman spectrum, which is an accumulation of all the Raman scattering in the entire laser excitation time $1/(2f_0)$, $I(\omega)$ is integrated over the laser excitation time $1/(2f_0)$. To simplify the analysis, the accumulative Raman signals are averaged by the laser excitation time $1/(2f_0)$ as

$$\overline{I} = 2A_0 f_0 \int_0^{1/(2f_0)} (1 - A\overline{\theta}_{nor}) e^{-4\ln 2[x-(\omega_0 - B\overline{\theta}_{nor})]^2/(\Gamma_0 + C\overline{\theta}_{nor})^2} dt \qquad (4)$$

By substituting the parameter $\overline{\theta}_{nor}$ with equation (2), the full expression of $\overline{I}(\omega, f_0)$ can be obtained. Based on the above equation, the theoretical Raman spectrum at different modulation frequencies can be calculated. By fitting the Raman intensity, Raman wavenumber, and linewidth against modulation frequency, the thermal diffusivity α can be determined. The large noise in the experimental data of linewidth makes the determination of thermal diffusivity less accurate. Consequently, only Raman intensity and Raman wave number are used to determine the thermal diffusivity α.

In the fitting process, the initial values of A, B, C are obtained from the experimental data directly as $A=2(I_{qs}-I_s)/(2I_{qs}-I_s)$=0.3293, $B=2(\omega_{qs}-\omega_s)$=3.2 cm^{-1}, $C=2(\Gamma_s-\Gamma_{qs})$=1.16 cm^{-1} when we compare the data at very low and very high modulation frequencies. Since B and C are the total variation of Raman wavenumber and linewidth from the steady state with a temperature rise of θ to the room temperature, the value of ω_0 and Γ_0 corresponding to room temperature is given by ω_s+B and Γ_s-C as ω_0=520.78 cm^{-1} and Γ_0=10.42 cm^{-1} respectively. However, as our lower and upper limit frequencies are not sufficiently low and high, the above values of these parameters deviate from their real values a little bit. As a result, to obtain the thermal diffusivity under the best fitting condition, the values of these parameters should be refined within a small range. Theoretically, f can be further increased to achieve a converged state. However, at high modulation frequencies, the heat conduction in the cantilever will have prominent 2D effect due to the ~μm-thick volumetric laser absorption at the cantilever surface.

In theory, all these parameters should be refined to approach their real values in the fitting process. C and Γ_0 are not refined due to their very low sensitivity to the temperature rise. B and ω_0 characterize the Raman wave number and are independent from each other: B determines the overall change of the Raman wave number, and ω_0 determines the absolute level of Raman wave number. In the fitting process, for each B, one best ω_0 can be quickly identified to minimize the difference between fitting and experimental data. Similarly, A_0 and A are independent from each other: A_0 determines the absolute level of the Raman intensity, and A gives the relative change. A_0 can be determined by one-step calculation to make the theoretical data best fit the experimental results. So, in fact only A and B are refined in the fitting process. The sensitivity of these parameters is not the same in different fitting process. To fit the change of the Raman wavenumber against f, B is the major parameter determining the fitting condition while A is much less sensitive in the fitting process. In fitting the peak intensity variation against f, A is very sensitive, but B becomes less important. The thermal diffusivity α determines how fast/slow the fitted properties change with f, is scanned from 1.01×10^{-5} m^2/s to 18×10^{-5} m^2/s with an increment of 1% each step. The discrepancy between the experimental data and the theoretical values is evaluated using the least square method.

The refined A and B obtained from the experimental Raman intensity is A_{int} and B_{int}, and the refined A and B from the experimental Raman wavenumber is A_{fre} and B_{fre}. Ideally we should have $A_{int}=A_{fre}$ and $B_{int}=B_{fre}$. However, this is impossible in real due to experimental errors. A is sensitive to the variation of Raman intensity, and B is sensitive to the change of Raman wavenumber. A_{int} and B_{fre} are used as the final values of A and B to extract thermal diffusivity α. Finally, we have A_{int}=0.33 and B_{fre}=3.3. For the Raman intensity, thermal diffusivity α is determined as 9.57×10^{-5} m^2/s (Fig. 4). To show the 10% uncertainty in the fitting result, the blue curve with a thermal diffusivity of 8.61×10^{-5} m^2/s and the green one with a thermal diffusivity of 10.53×10^{-5} m^2/s are plotted as shown in Fig. 4. Figure 4 also shows the best fitting curve to the experimental data of Raman wavenumber and its thermal diffusivity α is 11.00×10^{-5} m^2/s. To display the difference from the best fitted curve, a 10% fitting uncertainty of thermal diffusivity α is also plotted by the green curve and the blue curve. From Fig. 4, it can be observed that the fitting curve with 10% uncertainty can be readily distinguished from the best fitting curve. Accuracy and physics of the fitted thermal diffusivity are discussed later.

In addition to the Raman intensity, frequency and linewidth, the total Raman peak area is another important parameter that can be employed to characterize temperature rise. This peak area reflects the total Raman emission over the whole peak range of Raman wavenumber. At any instant, the Raman emission is a function of the temperature. The total Raman emission is the integral of each transient Raman emission in the total laser excitation time $1/(2f_0)$. To relate the experimental data with the theoretical total Raman emission, the total Raman emission is averaged by $1/(2f_0)$ as

$$E_{total} = A_e^{'} \int_0^{1/(2f_0)} (1 - A_e \overline{\theta}_{nor}) dt \quad (5)$$

where A_e is the total variation of the normalized total Raman emission from the steady state to the room temperature state. $A_e^{'}$ is a multiple relating the normalized theoretical data to the experimental data. When this function is employed to fit the experimental data, the fitting result is determined by A_e and α. (A_e is fitted directly rather than refined). The fitting process of total Raman emission is similar to that of the Raman intensity and frequency. To obtain the best fitting result, A_e is scanned from 5×10^{-3} to 1 with an increment of 5×10^{-3} every step and α is scanned form 10^{-5} m^2/s to 18×10^{-5} m^2/s with an increment of 1% every step. The best fitting result to the experimental data is illustrated by a red curve with the value of A_e and α as 0.295 and 9.02×10^{-5} m^2/s (Fig. 4). A_e is a little smaller than A (for Raman peak intensity) since the linewidth broadens with temperature rise. The advantage of this method is that it is an easy and convenient way to determine thermal diffusivity with a relative high accuracy. It avoids the time-consuming process of extracting Raman intensity, frequency and linewidth from reconstructed theoretical Raman spectrum.

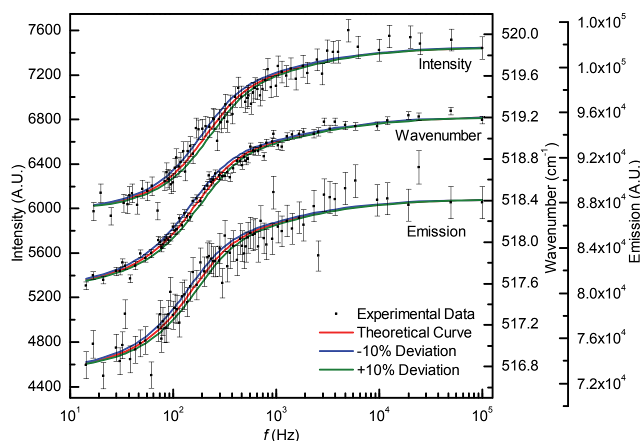

Fig. 4 The variation of Raman intensity, Raman wavenumber, and total Raman emission against *f*.

To evaluate the accuracy of the FR-Raman in thermal characterization, estimation of the thermal diffusivity in the physical model is of great importance. Since the thermal diffusivity is a temperature-dependent property, its value can be obtained by estimating the temperature rise of whole Si cantilever, then finding the reference value based on this temperature. As mentioned above, the Si cantilever tip at the steady state has a maximum temperature rise θ_s. θ_s can be calculated by $q=kA\theta_s/L$. q is the absorbed laser power which is the product of the incident laser power and the absorbance of single crystal Si (0.626 at 532 nm). k is the thermal conductivity of bulk Si. The value of k used in the calculation is 148 W/m·K at 300K [10]. A is the cross-section area of Si cantilever. Finally we have θ_s=56.98 K. By applying the relation $\theta_{qs}=\theta_s/2$, the spatially averaged temperature rise of Si cantilever tip at the quasi-steady state is 28.49 K. Thus, the spatially averaged temperature rise of Si cantilever tip is in a range of 28.49~56.98 K. From the Si cantilever tip to its end connected to chip, there is a temperature gradient along the axial direction, where the temperature rise decreases from θ to 0 K. As a result, the spatially averaged temperature rise of the whole Si cantilever θ_{avg} is between 14.25 K and 28.49 K. Since the experiment is performed at the room temperature (293 K), the absolute average temperature of Si cantilever is between 307.25 K and 321.49 K. The reference thermal diffusivity of single crystal Si is 8.66×10^{-5} m^2/s at 307.25 K and 8.16×10^{-5} m^2/s at 321.49 K respectively [10]. We can conclude that the thermal diffusivity of Si cantilever in the experiment should be between 8.16×10^{-5} m^2/s and 8.66×10^{-5} m^2/s.

Our measured thermal diffusivities are a little larger than the above estimated reference range. Such deviation can be explained by the thermal stress-induced variation in Raman spectrum. The non-uniform temperature distribution along the cantilever will induce a stress in it, along with some cantilever deflection. Under an increasing thermal stress and cantilever deflection, the Raman spectrum shows a decreasing intensity, a redshift of Raman wavenumber and a broadening linewidth. Such variation is similar to that induced by the increase of temperature. The variation of Raman spectrum obtained in the experiment is under the combined effect of both temperature rise and thermal stress. As a result, the properties of the Raman spectrum will have a larger and faster change against *f*, leading to an increased thermal diffusivity by data fitting. This type of effect can be mediated by using a higher sensitivity spectrometer that requires a lower excitation laser for Raman signal excitation. The thermal radiation and convection effect in the determined thermal diffusivity of the cantilever can be estimated as $(8\varepsilon\sigma T_0^3 + 4h)L^2/(\rho c_p \delta\pi^2)$ [11,12]. ε is the emissivity (< 0.1) of bulk Si at room temperature. h is the free convection coefficient, which is about 1~2 W/m^2·K at 300K. The thermal radiation and convection effect give a negligible error of ~4.8×10^{-8} m^2/s in the determined thermal diffusivity.

In summary, a frequency-resolved Raman technique was developed for measuring the thermal diffusivity of materials. A microscale Si cantilever was characterized to evaluate the capacity of the FR-Raman. A physical model was developed for the frequency-domain thermal transport and for Raman spectrum reconstruction based on temperature evolution. The variation of Raman intensity, wavenumber and emission (area under Raman peak) against f was fitted to determine the thermal diffusivity of Si cantilever. The measured thermal diffusivities are slightly higher than the reference value of Si due to the existence of thermal stress. Nonetheless, this new technique features significant advantage over the TD-Raman in terms of probing very fast transient thermal transport at the scale of μs to ns, and provides sufficient signal-to-noise ratio for sound data processing.

Funding. DOE (DENE) (0000671); National Natural Science Foundation of China (51428603), "Chutian" Scholar program of Hubei Province, China.

References

1. D. G. Cahill, K. E. Goodson, and A. Majumdar, J. Heat Transfer: Trans. ASME **124**, 223 (2002).
2. J. R. Serrano and S. P. Kearney, J. Heat Transfer **130**, 122401 (2008).
3. T. Beechem, S. Graham, S. P. Kearney, L. M. Phinney, and J. R. Serrano, Rev. Sci. Instrum. **78**, 061301 (2007).
4. Y. N. Yue, X. W. Chen, and X. W. Wang, ACS Nano **5**, 4466 (2011).
5. X. D. Tang, S. Xu, and X. W. Wang, Opt. Express **21**, 14303 (2013).
6. X. D. Tang, S. Xu, and X. W. Wang, Plos One **8**, e58030 (2013).
7. A. A. Balandin, S. Ghosh, W. Z. Bao, I. Calizo, D. Teweldebrhan, F. Miao, and C. N. Lau, Nano Lett. **8**, 902 (2008).
8. S. S. Chen, Q. Z. Wu, C. Mishra, J. Y. Kang, H. J. Zhang, K. J. Cho, W. W. Cai, A. A. Balandin, and R. S. Ruoff, Nat. Mater. **11**, 203 (2012).
9. S. Xu, T. Y. Wang, D. Hurley, Y. N. Yue, and X. W. Wang, Opt. Express **23**, 10040 (2015).
10. T. L. Bergman, F. P. Incropera, A. S. Lavine, and D. P. DeWitt, *Fundamentals of Heat and Mass Transfer* (John Wiley & Sons, 2011).
11. H. Lin, S. Xu, X. W. Wang, and N. Mei, Nanotechnology **24**, 415706 (2013).
12. G. Q. Liu, H. Lin, X. D. Tang, K. Bergler, and X. W. Wang, J. Visualized Exp. e51144 (2014).

References (With the title of paper)

1. D. G. Cahill, K. E. Goodson, and A. Majumdar, "Thermometry and thermal transport in micro/nanoscale solid-state devices and structures," J. Heat Transfer: Trans. ASME **124**, 223 (2002).
2. J. R. Serrano and S. P. Kearney, "Time-resolved micro-Raman thermometry for microsystems in motion," J. Heat Transfer **130**, 122401 (2008).
3. T. Beechem, S. Graham, S. P. Kearney, L. M. Phinney, and J. R. Serrano, "Invited Article: Simultaneous mapping of temperature and stress in microdevices using micro-Raman spectroscopy," Rev. Sci. Instrum. **78**, 061301 (2007).
4. Y. N. Yue, X. W. Chen, and X. W. Wang, "Noncontact sub-10 nm temperature measurement in near-field laser heating," ACS Nano **5**, 4466 (2011).
5. X. D. Tang, S. Xu, and X. W. Wang, "Thermal probing in single microparticle and microfiber induced near-field laser focusing," Opt. Express **21**, 14303 (2013).
6. X. D. Tang, S. Xu, and X. W. Wang, "Nanoscale probing of thermal, stress, and optical fields under near-field laser heating," Plos One 8, e58030 (2013).
7. A. A. Balandin, S. Ghosh, W. Z. Bao, I. Calizo, D. Teweldebrhan, F. Miao, and C. N. Lau, "Superior thermal conductivity of single-layer graphene," Nano Lett. **8**, 902 (2008).
8. S. S. Chen, Q. Z. Wu, C. Mishra, J. Y. Kang, H. J. Zhang, K. J. Cho, W. W. Cai, A. A. Balandin, and R. S. Ruoff, "Thermal conductivity of isotopically modified graphene," Nat. Mater. **11**, 203 (2012).
9. S. Xu, T. Y. Wang, D. Hurley, Y. N. Yue, and X. W. Wang, "Development of time-domain differential Raman for transient thermal probing of materials," Opt. Express **23**, 10040 (2015).
10. T. L. Bergman, F. P. Incropera, A. S. Lavine, and D. P. DeWitt, *Fundamentals of Heat and Mass Transfer* (John Wiley & Sons, 2011).
11. H. Lin, S. Xu, X. W. Wang, and N. Mei, "Significantly reduced thermal diffusivity of free-standing two-Layer graphene in graphene foam," Nanotechnology **24**, 415706 (2013).
12. G. Q. Liu, H. Lin, X. D. Tang, K. Bergler, and X. W. Wang, "Characterization of thermal transport in one-dimensional solid materials," J. Visualized Exp. e51144 (2014).